Iraqi Journal of Physics, 2022 *Vol.20, No. 3, PP.50-63*

DOI: 10.30723/ijp.v20i3.1026

P-ISSN: 2070-4003
E-ISSN: 2664-5548

Positron Interactions with Some Human Body Organs Using the Monte Carlo Probability Method

Zaheer S. Mohammad [1a], Jamal M.R. Abda [1b*]

[1]*Department of Physics, College of Science, University of Sulaimani, Sulaymaniyah, Iraq*

[a]E-mail: Zaheer.mohammad@univsul.edu.iq

[b*]Corresponding Author: jamal.abda@univsul.edu.iq

Abstract

In this study, mean free path and positron elastic-inelastic scattering are modeled for the elements hydrogen (H), carbon (C), nitrogen (N), oxygen (O), phosphorus (P), sulfur (S), chlorine (Cl), potassium (K) and iodine (I). Despite the enormous amounts of data required, the Monte Carlo (MC) method was applied, allowing for a very accurate simulation of positron interaction collisions in live cells. Here, the MC simulation of the interaction of positrons was reported with breast, liver, and thyroid at normal incidence angles, with energies ranging from 45 eV to 0.2 MeV. The model provides a straightforward analytic formula for the random sampling of positron scattering. ICRU44 was used to compile the elemental composition data. In this work, elastic cross sections (ECS) and inelastic cross-sections (ICS) for positron interaction in human tissues were studied. The elastic scattering is obtained from the Rutherford differential cross-section. Gryzinski's excitation function is used within the first-born approximation to determine the core and valence of ICS. The results are presented graphically. The ECS increases rapidly as the scattering energy approaches zero and becomes dependent on the atomic number of elements in organs. The ICS has reached a maximum value of around 100 eV. Increasing positron energy leads to an increase in the elastic and inelastic mean free paths. The simulations agree with many other studies dealing with the same parameters and conditions.

Article Info.

Keywords:
Positron interaction, Rutherford cross-section, Gryzinski excitation function, Mean free path, Human organ.

Article history:
Received: Jul. 4, 2022
Accepted: Aug. 14, 2022
Published: Sep. 01,2022

1. Introduction

Positron interactions with matter play a crucial role in explaining matter formation and lead to the highly relevant study of distinct physical processes. There are many applications of positron scattering cross-section that range from the study of medication to the characterization of materials, such as positron emission tomography (PET)[1] and radiation-induced corruption of biological organizations at the molecular level[2]. Accordingly, the knowledge of elastic and inelastic calculation for biological compounds is also effective. Many researchers have established several modeling studies on biological targets[3-7].

Charged particles are categorized into light-charged particles, such as positrons and electrons, and heavy-charged particles, such as alpha, deuteron, and protons. Each category interacts differently with bio-materials depending on their dissimilar masses[8]. The main mechanism for slowing down a traveling charged particle is their interactions with the electrons of the absorbing medium. These are Coulomb interactions known as elastic and inelastic collisions. Both collisions establish essential contributions to the transport process[9]. The act of each collision should be identified precisely for a decisive Monte Carlo simulation of such cases. Microscopic collisions of charged particles as many-body problems cannot be solved

accurately[10], and enough of the theories apply to several assumptions and approximations. The Monte Carlo estimates are an excellent method for analyzing the particle transport in matter[11].

The Monte Carlo approach has been broadly confirmed as one of the regularly required methods for investigating the penetration of energetic positrons and electrons in solids[12, 13]. In this method, the individual particle trajectories from a sequence of random scattering events are modeled as random steps and simulated on the computer. It is completely appreciated that the accuracy of the Monte Carlo method is firmly associated with the modeling of the scattering processes, which depend on the particle energy operated in the simulation. The success or failure of the model depends on the three physical quantities related to every collision: the mean free path, the scattering angle, and the energy loss[14].

Before a positron is inserted into the absorber object, it goes through elastic and inelastic scattering events. Both elastic and inelastic scattering processes are used in measuring particle ranges, transmission, absorption, and backscattering probabilities [15-17]. Calculating scattering events requires employing mathematical expressions known as differential cross-sections. These cross-sections describe particles' force, energy, and direction transitions when either driven toward the target or scattered away[18]. The major processes are the elastic scattering of individual atoms. Particles subjected to contact due to an elastic collision do not experience any changes to the internal structure of their bodies. However, the structures of particles carrying a little mass go through transformations that lead to movement. In an inelastic interaction, the target atom is either ionized or excited to a level that is suitably higher than the ground level, depending on how much power the reaching particle transfers to the target atom. Again, the entering particle drops energy and flows off in a particular orientation from its direction. Hence, inelastic scattering contains the core and valance electron excitations and ionizations[19, 20]. Significantly, instead of cross-sections, mean free paths (MFPs), which are fairly important, can also represent the scattering probability. For instance, the inelastic mean free path (IMFP) is critical since it represents the sufficient path length that a positron travels before it scatters inelastically, thereby losing some of its energy. In the case of human tissues, it influences the probability of damaging biomolecules[21].

Ionizing radiation in physics can take the form of charged particles or electromagnetic radiation. Charged particles may be produced using various isotopes and high-energy accelerators. Some radioactives, such as iodine, are used for treatment and diagnosis via beta-minus and gamma radiation[22]. The radiation composed of subatomic particles (electrons, positrons, and protons) interacts with matter at the level of the electron and the atomic nuclei. The interaction of radiation with biological compounds causes ionization or excitation of cells, leading to the breaking of chemical bonds. As a result, free radicals are formed that further ionize the cell, or direct damage to proteins, DNA and other cell components occurs[23]. The effectiveness of biological damage depends on the linear energy transfer (LET) value. It is also important to mention that the health impacts of ionizing radiation on humans and animals can emerge hours to weeks after exposure and can be positive or negative. The long-term consequences of exposure, such as cancer, death, and nerve function loss, may not be apparent for months or years[24, 25]. Therefore, there are strict limitations on the amount of ionizing radiation used to treat tumors due to the potential for damage to normal tissues and organs in the vicinity of a tumor[26, 27].

This paper presents the results of extensive Monte Carlo simulations of the slowing down of positrons on some human tissues, such as the breast, liver, and

thyroid, at energies ranging from 45 eV to 0.2 MeV. These tissues' essential components, concentrations, and densities were extracted from ICRU 44 (ICRU, 1989), as shown in Table 1. Herein, it includes both elastic and inelastic core-valence electrons scattering. It is shown that the calculated range is well saturated when the energy of the incident particle has weakened to a few electron volts in which the simulation array around these energies has been terminated. The elastic scattering cross-section was obtained from the Rutherford differential cross-section. The inelastic scattering model was employed to simulate the energy loss using Gryzinski's semi-empirical expression, which then calculated the mean free path of the incident positrons. Because the method described here contains mostly analytic expressions, interested readers can easily develop their method to calculate elastic, inelastic cross-sections, mean free path, and range for positrons in any target.

Table 1: Some human body tissues' elemental compositions and mass densities [28].

Tissues	Concentrations (%)										Mass density ($g.cm^{-3}$)
	H	C	N	O	Na	P	S	Cl	K	I	
Breast	10.6	33.2	3.0	52.7	0.1	0.1	0.2	0.1	-	-	1.02
Liver	10.2	13.9	3.0	71.6	0.2	0.2	0.3	0.3	0.3	-	1.06
Thyroid	10.4	11.9	2.4	74.5	0.2	0.1	0.1	0.2	0.1	0.1	1.05

2. Methods of calculations

The ideas of the Monte Carlo simulation have been described in calculations of keV positron and electron slowing down in solids (silicon, copper, and gold)[13]. In this research, the Monte Carlo technique was tested in the scattering process starting from 0.2 MeV positrons in a biological compound with considerable success. The models followed in traditional MC methods are based on the simulation of actual positron trajectories by assembling successive steps of a limited range. Each positron trajectory was simulated until it either backscattered from the surface or fell below 50 eV, at which point it was implanted or transmitted.

A positron is expected to flow in straight-line trajectories at each step with a finite length and constant energy with elastic scattering. Then, at the end of each step, the positron changes the direction of motion corresponding to the scattering formula of elastic scattering[29]. For inelastic scattering, it is assumed that the positron repeatedly loses its kinetic energy at each step length derived from the energy loss equation[30]. Gryzinski's excitation functions were used to describe both core and valance excitations in inelastic processes.

2.1. Elastic scattering

Many methods exist to address elastic scattering by a large number of atoms. The modified Rutherford differential scattering cross section is one convenient way. The differential scattering cross-section per atom $d\sigma_{el}$ is applied to define the elastic scattering of a positron-atom collision into a solid angle $d\Omega$ at a scattering angle θ as supported in[31]:

$$\frac{d\sigma_{el}}{d\Omega} = \frac{e^4 Z_i^2}{4E_p^2(1-cos\theta+2\beta_i)^2} \quad (1)$$

$$\beta_i = \frac{2.61 Z_i^{2/3}}{E_p} \quad (2)$$

where: Z_i is the atomic number of the i^{th} element, e is the electron charge, E_p is the incident positron energy in eV, θ is the scattering angle, and β_i is the atomic screening parameter to account for electrostatic screening of the nucleus by the orbital electrons. The total Rutherford scattering cross section can be obtained by using Eq.(1), as shown below:

$$\sigma_{el} = \frac{\pi e^4 Z_i^2}{4\beta_i(1+\beta_i)E_i^2} \quad (3)$$

2.2. Inelastic scattering

Both core and valence electron excitations were defined by Dym and Shames using Gryzinski's excitation function[32]. The differential cross-section of energy transfer E_p from a positron to an electron in the k^{th} inner shell is as follows:

$$\frac{d\sigma(\Delta E)}{d\Delta E} = \frac{\pi e^4}{(\Delta E)^3}\frac{E_B}{E_p}\left(\frac{E_p}{E_p+E_B}\right)^{\frac{3}{2}}\left(1-\frac{\Delta E}{E_p}\right)^{\frac{E_B}{E_B+\Delta E}} \times \left\{\frac{\Delta E}{E_B}\left(1-E_B/E_p\right)+\frac{4}{3}\,ln\left[2.7+\left(\frac{E_p-\Delta E}{E_B}\right)^{1/2}\right]\right\} \quad (4)$$

where: ΔE, E_B, and E_p are the energy losses, the mean electron binding energy, and the incident positron energy, respectively. For inelastic scattering, Gryzinski's excitation function yields the following total ionization cross-section:

$$\sigma_{inel} = \frac{\pi e^4 N_s}{E_p E_B}\left(\frac{E_p-E_B}{E_p+E_B}\right)^{\frac{3}{2}} \times \left\{1+\frac{2}{3}\left(1-\frac{E_B}{2E_p}\right)ln\left[2.7+\left(\frac{E_p}{E_B}-1\right)^{1/2}\right]\right\} \quad (5)$$

Here, N_s is the number of electrons in a particular "shell" that contributes to the inelastic events. Inelastic electron collisions do not take into consideration when the energy loss is less than the binding energy of electrons [see Eq.(5)]. The processes also have their role in positron stopping in an object, for example, a core electron excitation event between two atomic levels. From Eq.(4), the crude approximation happened rather than the excitation function and constant for small energy losses:

$$\left.\frac{d\sigma(\Delta E)}{d\Delta E}\right|_{\Delta E \le E_B} = \left.\frac{d\sigma(\Delta E)}{d\Delta E}\right|_{\Delta E = E_B} \quad (6)$$

The total inelastic scattering cross-section is given as follows:

$$\sigma_{inel} = \int_0^{E_p} \frac{d\sigma(\Delta E')}{d\Delta E'}\, d\Delta E' \quad (7)$$

At each inelastic scattering event, the energy loss is calculated by selecting a uniform random number R_1 and then finding a value of ΔE that satisfies:

$$\boldsymbol{R_1 = \int_{\Delta E}^{E_p} \frac{d\sigma(\Delta E')}{d\Delta E'} d\Delta E' / \sigma_{inel}} \quad \textbf{(8)}$$

$$\boldsymbol{R_1 = E_B^2 \left(\frac{E_p}{E_p - E_B}\right)^{\frac{3}{2}} \int_{\Delta E}^{E_p} \frac{1}{(\Delta E)^3} \left(1 - \frac{\Delta E}{E_p}\right)^{\frac{E_B}{E_B + \Delta E}} \left\{\frac{\Delta E}{E_B}\left(1 - \frac{E_B}{E_p}\right) + \frac{4}{3} ln[2.7 + \sqrt{\frac{E_p - \Delta E}{E_B}}]\right\} \times \left\{1 + \frac{2}{3}\left(1 - \frac{E_B}{2E_p}\right) ln[2.7 + \sqrt{\frac{E_p}{E_B} - 1}]\right\}^{-1} d\Delta E} \quad \textbf{(9)}$$

From the equation, ΔE values that satisfy $0 \leq R_1 \leq 1$ can be obtained; after finding ΔE, which may be greater than E_B or $\Delta E > E_B$; otherwise, $\Delta E = 0$.

2.3. Positron motion in human organ

In this model, the mean free path of the penetrating particle is given by:

$$\boldsymbol{\lambda = \frac{A}{N_A \rho \sigma}} \quad \textbf{(10)}$$

where: A, N_A, ρ and σ are the atomic mass, the Avogadro number, the mass density, and the collision cross-section, respectively. The value of the mean free path depends on the material target and positron energy[33]. The inverse of the total mean-free path λ_T is a sum of the different processes:

$$\boldsymbol{\frac{1}{\lambda_T} = \frac{1}{\lambda_{el}} + \frac{1}{\lambda_c} + \frac{1}{\lambda_v}} \quad \textbf{(11)}$$

where: λ_{el} is the elastic mean free path and λ_c and λ_v are associated with core and valence electron excitations (inelastic mean free path), respectively. The distance traveled between collisions (S) is then:

$$\boldsymbol{S = -\lambda_T ln R_2} \quad \textbf{(12)}$$

where: R_2 is a uniform random number. A third random number R_3 is used to determine whether a scattering event was elastic or inelastic. Satisfaction of this inequality implied that an elastic event had occurred and R_3 was further used to determine which atomic species acted as the scattering center. However, if the inequality was not satisfied, an inelastic event occurred, and the type of inelastic event was determined by using[31]

$$\boldsymbol{R_3 \leq \frac{1/\lambda_{el}}{1/\lambda_T}} \quad \text{elastic scattering}$$

$$\boldsymbol{\frac{1/\lambda_{el}}{1/\lambda_T} < R_3 \leq \frac{1/\lambda_{el} + 1/\lambda_c}{1/\lambda_T}} \quad \text{core-electron excitation}$$

$$\boldsymbol{\frac{1/\lambda_{el} + 1/\lambda_c}{1/\lambda_T} < R_3 \leq 1} \quad \text{valence electron excitation}$$

After choosing the scattering type, the energy loss in an inelastic collision was computed.

3. Result and discussion

This work reports the calculations of incident positrons in breast, liver, and thyroid tissues. The material composition and mass densities of the tissues were taken

from Table 1. The results for elastic, inelastic (core and valence) cross-section, and mean free path at incident energies between 45 eV to 0.2 MeV have been collected. The positron interaction with an electron in tissues was used in various experimental and clinical applications, such as positron emission tomography in the heart for the measurements of blood flow[34] and imaging to personalize esophagogastric cancer care[35].

Fig.1 shows the change of elastic cross-sections as a function of the incident positron energies (from 0 to 5 keV) for the three human organs. It can be seen from the figure that the minimum elastic cross-section (1.35×10^{-20} m^2) in all organs at low incident energy, 45 keV, was almost recorded for hydrogen (H). At the same time, an implanted positron produces a distinct effect in each organ due to their composition (see Table 1). Maximum elastic cross-sections for chloride (Cl), potassium (K), and iodide (I) have been measured at 44×10^{-20} m^2, 51×10^{-20} m^2, and 157×10^{-20} m^2 in the breast, liver, and thyroid, respectively. Iodine (Z=53) was found to have the highest elastic cross-section compared to chloride (Z=17) and potassium (Z=15) since atomic number affects the cross-section in this way (see Eq. (3))[36]. In contrast, there does not seem to be a significant change in the elastic cross-section of components over 5keV. At high positron energy, the elastic cross-section rapidly declines to zero. The present elastic cross-section data shows good agreement with the results from Pimblott et al. and Champion et al. that were previously reported[37, 38].

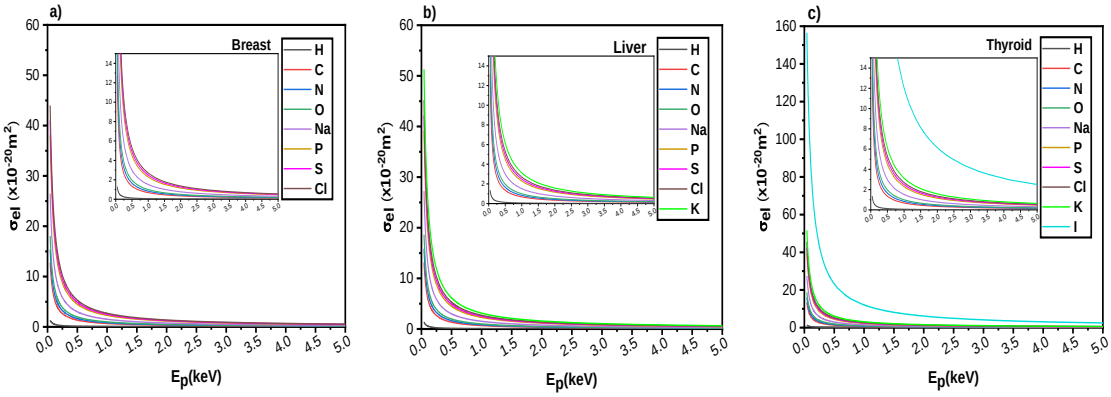

Figure 1: Elastic cross-section as a function of positron energy for (a) breast, (b) liver, and (c) thyroid.

Figs. 2 and 3 show the dependency of the inelastic core and valence cross-sections of the three tissues on the incoming positron energy from 0 to 5 keV, and 2 keV, respectively. Fig.2 shows that the values of the inelastic core cross-section of the components in each of the three human bodies differ. At low incident energy of 75 eV, oxygen causes the inelastic core cross-section to be at its lowest of 0.26×10^{-20} m^2 in all three tissues. However, phosphorus (P), potassium (K), and iodide (I) were responsible for the maximum inelastic core cross-sections in the breast (3.5×10^{-20} m^2), liver (4.2×10^{-20} m^2) and thyroid (14×10^{-20} m^2). Fig.3 shows the inelastic valence cross-sections of the three organs, which were similar with slight differences in the rates of individual elements. Hydrogen (H) also takes all tissues' lower limit inelastic valence cross-section (0.7×10^{-20} m^2). However, sulphate (S) has the maximum inelastic valence cross-section (7.5×10^{-20} m^2) for the breast and liver, and iodide (I) has the maximum value (20.8×10^{-20} m^2) in the thyroid. The inelastic core and valence cross-section depend on the binding energy and the number of electrons in a particular shell.

The ion cores are also more attractive if the number of core and valence electrons per atom is high[12].

Up until around 100 eV, the inelastic core cross-section increased as the positron energy increased. Fig.2 shows that the probability of positrons interacting with electrons in the inner shell was higher at that energy. It was estimated that the probability of inelastic core scattering was around half that of inelastic valence scattering. At approximately 100 eV, the maximum positron energy loss rate occurred in valence ICS. This means that it has the largest probability of scattering in tissues and slowing down thermal energies. Notably, our determination of inelastic cross-section values agrees with those published by Dingfelder et al. and Emfietzoglou et al.[39, 40].

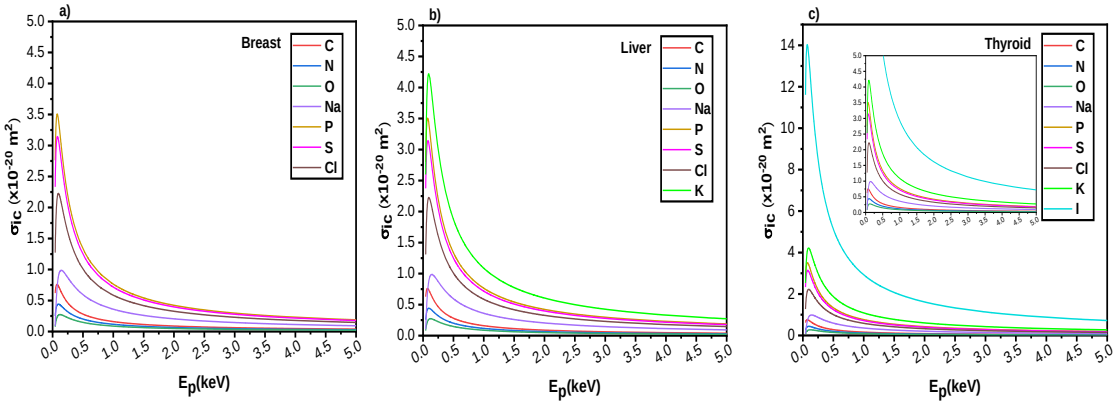

Figure 2: Inelastic core cross-section as a function of positron energy for (a) breast, (b) liver, and (c) thyroid.

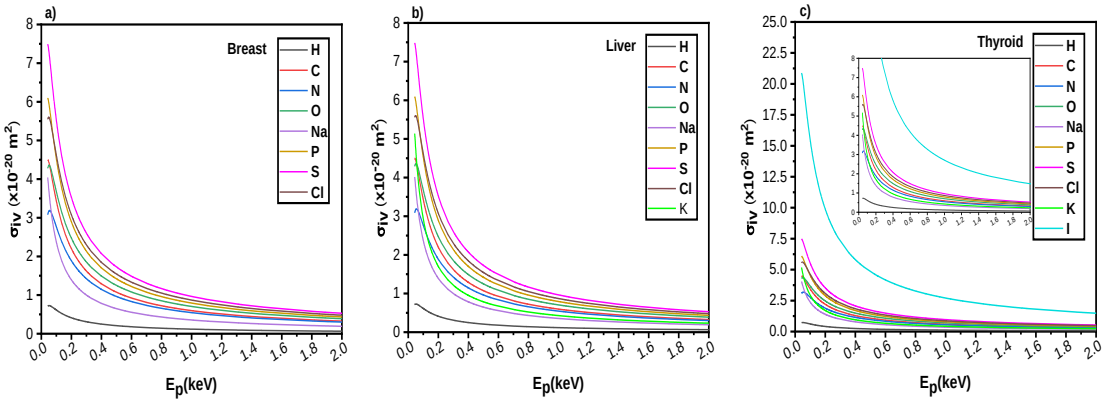

Figure 3: Inelastic valence cross-section as a function of positron energy for (a) breast, (b) liver, and (c) thyroid.

The elastic mean free path theory is essential to predict radioactivity effects on biological compounds since it assists in distances between collisions. Inelastic mean free path plays a significant character in physics surfaces at small incident energies [41]. Fig. 4 shows the elastic mean free path as a function of positron energy at the normal incident for the breast, liver, and thyroid. The measured elastic mean free paths of carbon in the three tissues were the largest values. It has a value of 5.5×10^{-7} m at 200 keV. In contrast, the minimum elastic mean free paths were 4.1×10^{-7} m for sulfate, 3.8×10^{-7} m for potassium, and 3.2×10^{-7} m for iodide at the same energy point in the breast, liver, and thyroid, respectively. However, these tissues' elastic mean free paths for hydrogen (H) and oxygen (O) were the same.

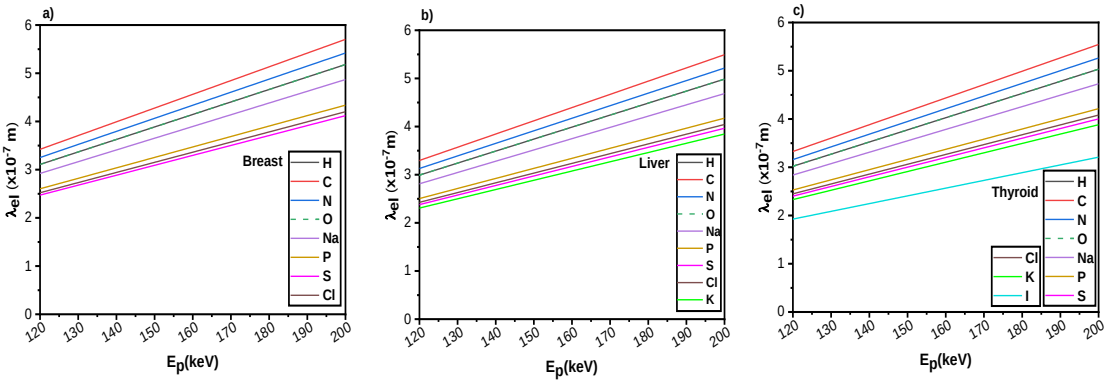

Figure 4: Elastic mean free path as a function of positron energy for (a) breast, (b) liver, and (c) thyroid.

Figs. 5 and 6 show the plotted inelastic mean free paths versus incident positron energy (from 120 to 200 keV) for the two types, core, and valence. As can be seen in Fig.5, the minimum value of inelastic core mean free path at high positron energy (200 keV) was achieved for phosphor (7.6×10^{-7} m) in the breast, potassium (6.4×10^{-7} m) in the liver, and thyroid. However, the maximum inelastic core mean free path was for oxygen (greater than 31.4×10^{-7} m) for the three organs. In addition, the inelastic core mean free path of sodium (Na) and chloride (Cl) have the same value (11.1×10^{-7} m). On the other hand, a plot of the inelastic valence mean free path against incoming positron energy (from 120 to 200 keV) is shown in Fig.6. From this, one can notice that the inelastic valence mean free path for hydrogen (H) at high positron energy (200 keV) is a minimum value of 1.55×10^{-7} m in the three organs. At that point, the maximum value for sodium (Na) was (12.9×10^{-7} m) in the breast, and in the liver with thyroid organs, potassium (K) recorded the maximum value (17.7×10^{-7} m). The elastic and inelastic mean free path parameters depend on the elements and the positron energy [33]. Some reports indicate that the inelastic mean free path for incident positron takes energies between 50 eV-200 keV for liquid, organic, and inorganic compounds[42-44].

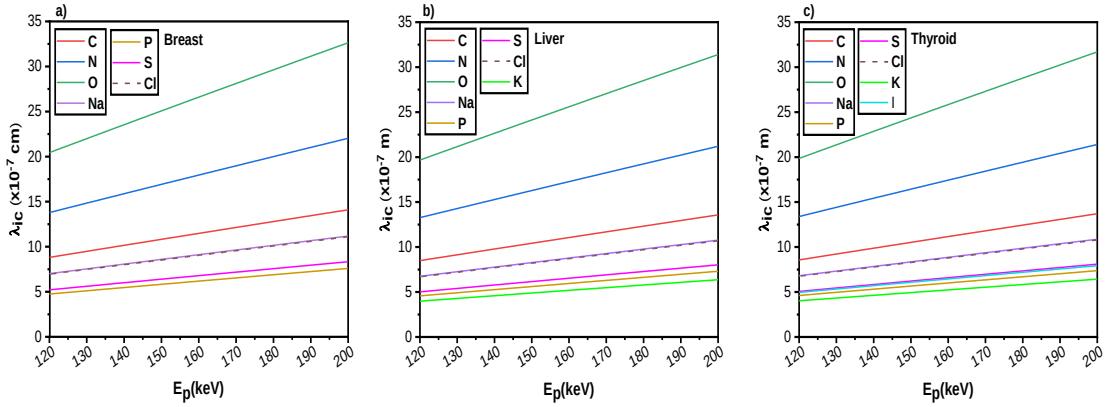

Figure 5: Inelastic core mean free path as a function of positron energy for (a) breast, (b) liver, and (c) thyroid.

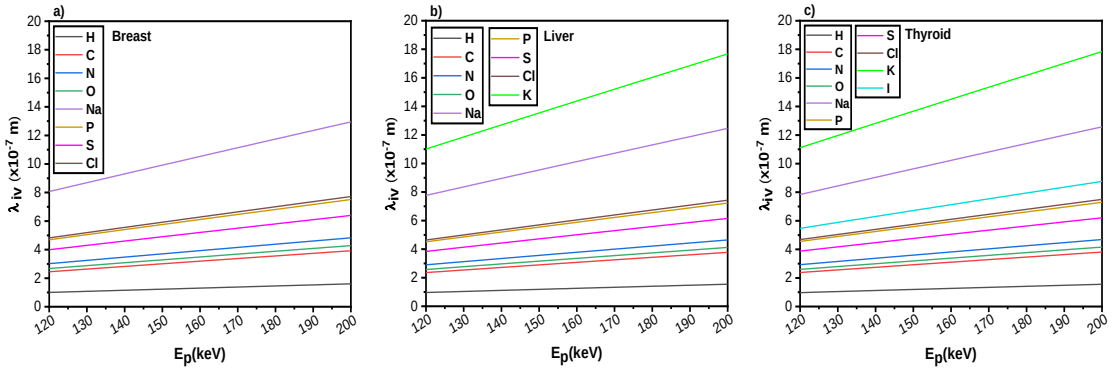

Figure 6: Inelastic valence mean free path as a function of positron energy for (a) breast, (b) liver, and (c) thyroid.

The implications of these results are stated clearly from a clinical and medical point of view by these images, which show elastic and inelastic cross sections. Higher cross sections indicate more significant impacts from interactions with a specific organ's components. Therefore, the damage is more significant, particularly for the thyroid and valence values, which are nearly twice as large as the core inelastic cross section. Special devices are used to measure this during a PET scanner, which uses scintillation detectors as its detection elements. Its values for the mean free path inelastic core are approximately five times that of elastic values, and for valence mean free paths, it is twice the value. This indicates the danger of exposure to these particles at these energies, as the more positron particles enter, the more dangerous their effects will be.

4. Positron simulation flowchart

The computer modeling simulation program of incident positron energy of 0.2 MeV in three specific human organs has been written in a slab of 4 μm^2 area. A liver example has been selected for the positron trajectories to show this modeling's characteristics and possible applications. Herein, the backscattered positron behaviour was neglected, while all positrons have backscattered or slowed down below 50 eV. For this purpose, a unique program modeling was laid out, as shown in Fig.7 (a). The Monte Carlo simulation procedure of a high-energy positron for the 100 and 1000 particles is shown in Fig.7 (b and c), in which the maximum penetration of positrons in the liver was less than 1 μm.

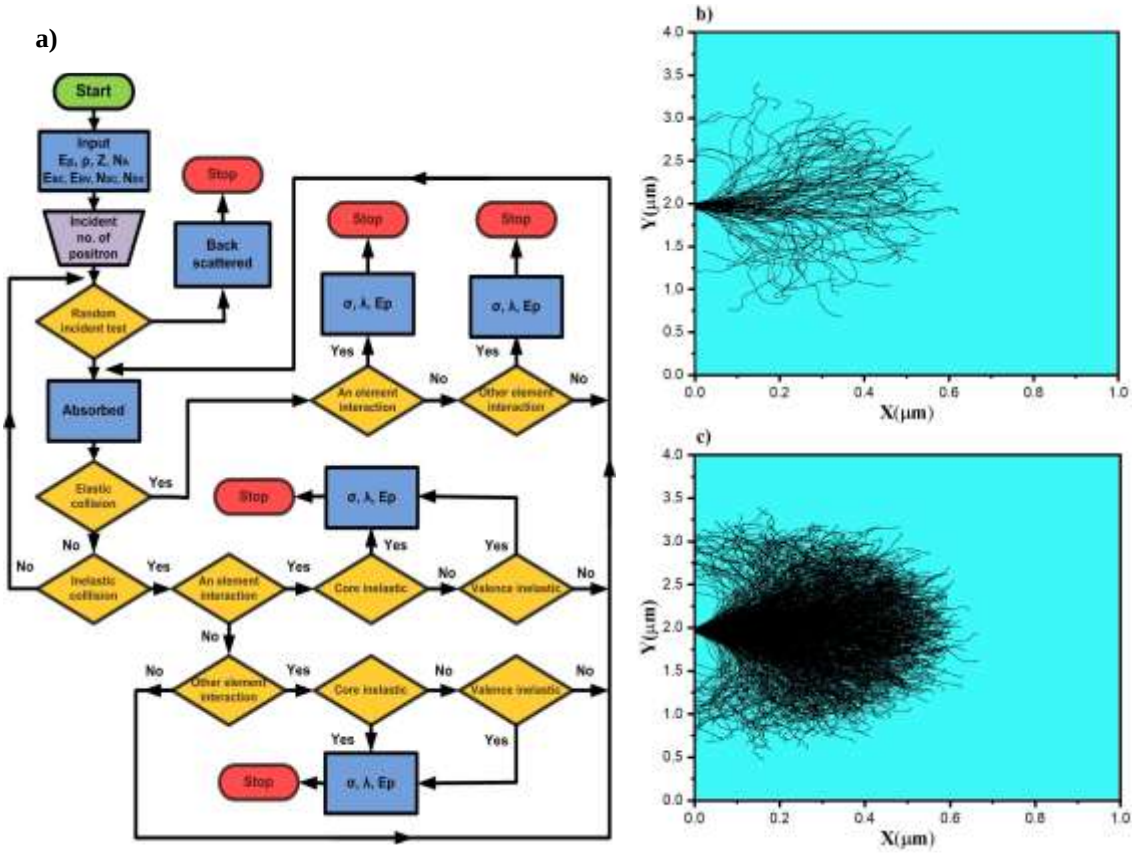

Figure 7: (a) Flow diagram of the modeling procedure: Backscattered and absorbed fractions of positrons, output, and feedback by Monte Carlo simulation for injection of (b) 100 particles and (c) 1000 particles for a liver organ, with 0.2 MeV particle energy.

5. Conclusions

The Monte Carlo technique was used to compute positron elastic-inelastic scattering along with the mean free path in the breast, liver, and thyroid. It was performed for positron incidence energies from 45 eV to 0.2 MeV using screened Rutherford differential cross-section and Gryzinski's excitation function. Minimal ECS in all organs at 45 eV incident energy was nearly recorded for hydrogen. The least core ICS was attributed to oxygen at incidence energy of approximately 75 eV, whereas hydrogen had the lowest valence ICS in all organs. ECS is related to positron energy and atomic number. The core-valence ICS is determined by the binding energy and the number of electrons in a given shell. In valence ICS, the positron energy loss rate peaked at around 100 eV. It is most likely due to scattering in tissues, reducing its speed to thermal energies. Furthermore, the elastic and inelastic mean free path parameters depend on elements and positron energy. The current ECS and ICS data agree well with published results, mainly in the 45- 120 eV. The result demonstrates the study's effectiveness and reliability. There is no difference between ECS and ICS values of elements for individual organ energies. This is important for planning dosage in radiation oncology and nuclear medicine. Moreover, the presented method is easily adaptable to any other target, whether compounded or not. The method employed here can only be applied to projectile positrons, electrons, and heavy-charged particles. In conclusion, the cross-section needs to be known precisely in order to calculate the patient's radiation dose.

Acknowledgement

The first author thanks the financial support of the Ministry of Education, Ministry of Higher Education, and Scientific Research of the Kurdistan Regional Government, and the authors indebted (Darko A. Noori) for his helpful and skillful technical assistance.

Conflict of interest

Authors declare that they have no conflict of interest.

References

1. Berg E. and Cherry S.R., *Innovations in instrumentation for positron emission tomography.* Seminars in nuclear medicine, 2018. **48**(4): pp. 311-331.
2. Singh S., Dutta S., Naghma R., and Antony B., *Theoretical formalism to estimate the positron scattering cross section.* The Journal of Physical Chemistry A, 2016. **120**(28): pp. 5685-5692.
3. Bert J. and Sarrut D., *Monte Carlo simulations for medical and biomedical applications.* Biomedical Image Synthesis and Simulation, 2022: pp. 23-53.
4. Garcia-Molina R., Abril I., Kyriakou I., and Emfietzoglou D., *Inelastic scattering and energy loss of swift electron beams in biologically relevant materials*. Surface Interface Analysis, 2017. **49**(1): pp. 11-17.
5. Stevens D., *Experiments in the application of positrons to medical physics*, MPhil Thesis, Australian National University, 2020.
6. Carter L.M., Kesner A.L., Pratt E., Sanders V., Massicano A., Cutler C., Lapi S., and Lewis J.S., *The impact of positron range on PET resolution, evaluated with phantoms and PHITS Monte Carlo simulations for conventional and non-conventional radionuclides.* Molecular Imaging Biology, 2020. **22**(1): pp. 73-84.
7. O'Doherty J., Mangini C.D., Hamby D.M., Boozer D., Singh N., and Hippeläinen E., *Estimation of absorbed radiation doses to skin and s-values for organs at risk due to nasal administration of PET agents using Monte Carlo simulations.* Medical Physics, 2021. **48**(2): pp. 871-880.
8. Mohammed S., Trabelsi A., and Manai K., *Stopping power, CSDA range, absorbed dose and cross sections calculations of f18 simulated in water using Geant4 code.* Indian Journal of Science Technology, 2018. **11**(6): pp. 1-10.
9. Chen J., Keane D., Ma Y.-G., Tang A., and Xu Z., *Antinuclei in heavy-ion collisions.* Physics Reports, 2018. **760**: pp. 1-39.
10. Zakharov A. Y. and Zubkov V. V., *Field-Theoretical Representation of Interactions between particles: Classical relativistic probability-free kinetic theory*," Universe, 2022. **8**(5), pp. 1-10.
11. Ma D., Yang B., Zhang Q., Liu J., and Li T., *Evaluation of single-node performance of parallel algorithms for multigroup Monte Carlo particle transport methods.* Frontiers in Energy Research, 2021. **9**: pp. 705823(1-12).
12. Liljequist D., *A simple calculation of inelastic mean free path and stopping power for 50 eV-50 keV electrons in solids.* Journal of Physics D: Applied Physics, 1983. **16**(8): pp. 1567-1582.
13. Valkealahti S. and Nieminen R., *Monte-Carlo calculations of keV electron and positron slowing down in solids.* Applied Physics A, 1983. **32**(2): pp. 95-106.
14. Aydın A., *Monte Carlo calculations of low energy positrons in silicon.* NUKLEONIKA, 2005. **50**(1): pp. 37−42.

15. Hussain A., Yang L., Mao S., Da B., Tőkési K., and Ding Z., *Determination of electron backscattering coefficient of beryllium by a high-precision Monte Carlo simulation.* Nuclear Materials Energy, 2021. **26**: pp. 100862(1-17).
16. Sinha N., Subraveti P., and Antony B., *Electron and positron backscattering from condensed targets.* Journal of Physics B: Atomic, Molecular Optical Physics, 2021. **54**(20): pp. 205001.
17. Yan Q., Meng X., Liu D., Zhang Q., and Zhu J., *Evaluation of displacement damage in solids induced by fast positrons: Modeling and effect on vacancy measurement.* Nuclear Materials Energy, 2021. **27**: pp. 101022(1-14).
18. Koç K. and Çetin A., *Investigation of interactions between low energy positrons and dna using the Monte-Carlo method.* Neuro Quantology, 2015. **13**(2): pp. 160-169.
19. Aydın A., *Monte Carlo calculations of electrons in aluminum.* Applied Radiation Isotopes, 2009. **67**(2): pp. 281-286.
20. Arretche F., Barp M.V., Seidel E.P., and Tenfen W., *Electronic excitation of H2O by positron impact.* The European Physical Journal D, 2020. **74**(1): pp. 1-7.
21. Sinha N. and Antony B., *Mean free paths and cross sections for electron scattering from liquid water.* The Journal of Physical Chemistry B, 2021. **125**(21): pp. 5479-5488.
22. Wyszomirska A., *Iodine-131 for therapy of thyroid diseases. Physical and Biological basis.* Nuclear Medicine Review, 2012. **15**(2): pp. 120-123.
23. Panetta T.F., Davila-Santini L.R., and Olson A., *Radiation physics and radiation safety, Endovascular Surgery E-Book.* 2010, ELSEVIER. p.27-40.
24. Nair C.K., Parida D.K., and Nomura T., *Radioprotectors in radiotherapy.* Journal of Radiation Research, 2001. **42**(1): pp. 21-37.
25. Jagetia G.C. and Reddy T.K., *Modulation of radiation-induced alteration in the antioxidant status of mice by naringin.* Life Sciences, 2005. **77**(7): pp. 780-794.
26. Mutter R.W., Choi J.I., Jimenez R.B., Kirova Y.M., Fagundes M., Haffty B.G., Amos R.A., Bradley J.A., Chen P.Y., and Ding X., *Proton therapy for breast cancer: A consensus statement from the particle therapy cooperative group breast cancer subcommittee.* International Journal of Radiation Oncology Biology Physics, 2021. **111**(2): pp. 337-359.
27. Kunwar A., Bansal P., Kumar S.J., Bag P., Paul P., Reddy N., Kumbhare L., Jain V., Chaubey R., and Unnikrishnan M., *In vivo radioprotection studies of 3, 3'-diselenodipropionic acid, a selenocystine derivative.* Free Radical Biology Medicine, 2010. **48**(3): pp. 399-410.
28. White D.R., Booz J., Griffith R.V., Spokas J.J., and Wilson I.J., *ICRU reports: Reports of the International Commission on Radiation Units and Measurements.* 1989. **os-23**(1): pp. 184-186.
29. Rutherford E., *The scattering of α and β particles by matter and the structure of the atom.* Philosophical Magazine, 2012. **92**(4): pp. 379-398.
30. Gryziński M., *Two-particle collisions. i. general relations for collisions in the laboratory system.* Physical Review, 1965. **138**(2A): pp. A305-A321.
31. Adesida I., Shimizu R., and Everhart T., *A study of electron penetration in solids using a direct Monte Carlo approach.* Journal of Applied Physics, 1980. **51**(11): pp. 5962-5969.
32. Dym C.L. and Shames I.H., *Classical theory of plates,* in *Solid Mechanics*. 2013, Springer. p. 299-372.
33. Powell C.J., *Practical guide for inelastic mean free paths, effective attenuation lengths, mean escape depths, and information depths in x-ray photoelectron*

spectroscopy. Journal of Vacuum Science Technology A: Vacuum, Surfaces, Films, 2020. **38**(2): pp. 023209(1-14).
34. Bohigian G.M., Estes E.H., Friedlander I.R., Kennedy W.R., Moxley J.H., Numann P., Salva P.S., Scott W.C., Skom J.H., and Steinhilber R.M., *Application of positron emission tomography in the heart.* JAMA, 1988. **259**(16): pp. 2438-2445.
35. Mondaca S. and Janjigian Y.Y., *Application of positron emission tomography imaging to personalize esophagogastric cancer care.* Cancer, 2019. **125**(8): pp. 1214-1217.
36. Lenz F., *Cross Sections of atoms for elastic and inelastic scattering of electrons.* Berichte der Bunsengesellschaft für physikalische Chemie, 1970. **74**(11): pp. 1187-1190.
37. Pimblott S.M., LaVerne J.A., and Mozumder A., *Monte Carlo simulation of range and energy deposition by electrons in gaseous and liquid water.* The Journal of Physical Chemistry A, 1996. **100**(20): pp. 8595-8606.
38. Champion C., Incerti S., Aouchiche H., and Oubaziz D., *A Free-parameter theoretical model for describing the electron elastic scattering in water in the geant4 toolkit.* Radiation Physics Chemistry of materials, 2009. **78**(9): pp. 745-750.
39. Dingfelder M., Hantke D., Inokuti M., and Paretzke H.G., *Electron inelastic-scattering cross sections in liquid water.* Radiation physics chemistry of materials, 1998. **53**(1): pp. 1-18.
40. Emfietzoglou D., Kyriakou I., Garcia-Molina R., Abril I., and Nikjoo H., *Inelastic cross sections for low-energy electrons in liquid water: exchange and correlation effects.* Radiation Research, 2013. **180**(5): pp. 499-513.
41. Aouina N.Y. and Chaoui Z.E.A., *Simulation of Positron and electron elastic mean free path and diffusion angle on DNA nucleobases from 10 eV to 100 keV.* Surface Interface Analysis, 2018. **50**(10): pp. 939-946.
42. Shinotsuka H., Tanuma S., Powell C.J., and Penn D.R., *Calculations of Electron Inelastic Mean Free Paths. XII. Data for 42 Inorganic compounds over the 50 eV to 200 keV range with the full penn algorithm.* Surface Interface Analysis, 2019. **51**(4): pp. 427-457.
43. Shinotsuka H., Da B., Tanuma S., Yoshikawa H., Powell C., and Penn D.R., *Calculations of electron inelastic mean free paths. XI. data for liquid water for energies from 50 eV to 30 keV.* Surface Interface Analysis, 2017. **49**(4): pp. 238-252.
44. Tanuma S., Powell C.J., and Penn D.R., *Calculations of electron inelastic mean free paths. V. Data for 14 organic compounds over the 50–2000 eV range.* Surface Interface Analysis, 1994. **21**(3): pp. 165-176.

تفاعلات البوزترون مع بعض أعضاء جسم الانسان باستخدام طريقة احتمالية المونت كارلو

زاهر محمد سعيد[1]، جمال محمد رشيد عبده[1]
[1]قسم الفيزياء، كلية العلوم، جامعة السليمانية، سليمانية، العراق

الخلاصة

في هذه الدراسة، تمت نمذجة متوسط المسار الحر والتشتت المرن والغير المرن للبوزترون لعناصر الهيدروجين (H) والكربون (C) والنيتروجين (N) والاوكسجين (O) والفوسفور (P) والكبريت (S) والكلور (Cl) والبوتاسيوم (K) واليود (I) في الاعضاء البشرية المنتقاة. على الرغم من الكميات الهائلة من البيانات المطلوبة، تم تطبيق طريقة مونت كارلو (MC)، مما يسمح بمحاكاة دقيقة للغايه لتصادم تفاعل البوزترون في الخلايا الحية. هنا، نقدم تقريراً عن محاكاة MC لتفاعل البوزترونات مع الصدر والكبد والغدة الدرقية بزوايا الوقوع الطبيعية، مع طاقات تتراوح من 45 اليكترون فولت الى 0.2 ميجا اليكترون فولت. يوفر النموذج صيغة تحليلية مباشرة لأخذ العينات العشوائي لتشتت البوزترون. تم استخدام ICRU44 لتجميع بيانات تكوين العناصر. تمت دراسة المقاطع العرضية المرنة (ECS) والمقاطع العرضية الغير المرنة (ICS) للتفاعل البوزتروني في الانسجة البشرية في هذا العمل. تم الحصول على الانتشار المرن من المقطع العرضي التفاضلي لرذرفورد. استخدمت دالة اثارة Gryzinski ضمن تقريب بورن الاول لحساب جوهر وتكافؤ ICS. تزداد ECS بسرعة مع اقتراب طاقة التشتت من الصفر وتصبح معتمدة على العدد الذري للعناصر في الاعضاء. وصلت قيمة ICS الى قيمة قصوى تبلغ حوالي 100 اليكترون فولت. تؤدي زيادة طاقة البوزترون الى زيادة متوسط المسار الحر المرن والغير المرن. تتفق عمليات المحاكاة مع العديد من الدراسات الاخرى التي تتعامل مع نفس العوامل والشروط.